Regular Article

Thermal energy harvesting system based on magnetocaloric materials[★]

Smail Ahmim[*], Morgan Almanza, Alexandre Pasko, Frédéric Mazaleyrat, and Martino LoBue

SATIE, ENS Paris-Saclay, CNRS, Université Paris-Saclay, 94235 Cachan, France

Abstract. We numerically study the design of a thermomagnetic generator aimed to convert a heat flow into electrical energy. The device uses the variation of magnetization of a magnetocaloric material (MCM) along a cyclic transformation between the hot and the cold sources. The magnetic energy is transformed into mechanical energy via the magnetic forces and eventually into electrical energy through an electromechanical transducer. Firstly, we work-out the optimal size of the cantilever in order to achieve the self-oscillation of the MCM between the two heat sources. Eventually, using finite element calculations, we compare the efficiency of a piezoelectric transducer (PZT 5a) with that of a set of coils in order to convert the mechanical into electrical energy. The piezoelectrics and the coils recover 0.025% and 0.018% respectively of the available mechanical energy $(116 \, \text{mJ/cm}^3)$. The possible strategies to achieve a better performance are discussed in the conclusion.

1 Introduction

Nowadays the number of connected systems is constantly increasing. Some of these systems are autonomous, often small (mm to cm), and require a source of energy. Low grade heat sources (i.e. temperature differences below 60 K) are quite ubiquitous [1] making thermal energy recovery systems the natural candidates for powering small autonomous devices.

Though thermoelectric generators can produce enough power to feed a microsystem (10 μW) [2], their performances can hardly be improved over reduced temperature gradients and small length scales and this motivates an increased research for alternative technologies [3]. The development of a new generation of magnetocaloric material (MCM) for refrigeration applications is offering some new opportunities to energy harvesting technologies. In cooling applications, the magnetocaloric effect is used to pump heat through the entropy change of the MCM associated to application/ removal of a field. Thermomagnetic generators (TMGs) use the pyromagnetic effect, namely the variation of magnetization as a function of the temperature, to perform thermodynamic cycles under varying field and eventually convert the magnetic into electrical energy.

Several thermo-generation prototypes using MCM have been realized so far. Recently, Ujihara and coworkers [3] realized a TMG showing an estimated electrical power density between 1.85 and 3.61 mW/cm^2 for a temperature difference between the hot and cold source of $\Delta T_{\text{res}} = 50$ K. Gueltig and coworkers from Karlsruhe [4] realized a

generator showing an electrical power density of 122 mW/cm^3 for $\Delta T_{\text{res}} = 140$ K using micro-coils to harvest the energy. As our theoretical calculations [5] show that for $\Delta T_{\text{res}} = 3$ K a magnetocaloric generator can produce up to 10 mW for 1 cm^3 of MCM, we have undertaken a detailed study of the different steps of the conversion chain in order to design a device getting closer to the theoretical prediction.

The energy conversion chain in a typical TMG is composed of three stages. The first is the heat to magnetic energy conversion through the temperature dependence of the magnetization in the proximity of a phase transition, the second uses the magnetic force from a permanent magnet to convert part of the energy change associated with the transition into mechanical energy, the third converts the mechanical energy into electrical energy. Whereas general thermodynamic considerations allow to work-out the efficiency of the thermal cycle, estimating the efficiency of the mechanical to electrical energy conversion can be a hard task, and it often relies on extrapolations from approximated models. In [3] for instance, a simple model has been used where the mechanical–electrical conversion efficiency is roughly estimated for a piezoelectric at resonance [6].

Nevertheless, an accurate modeling of the final conversion step represents a key input to device design. That is the main motivation of this work where we shall present the comparison of the two methods used in [3] and [4], piezoelectric and micro-coils, respectively, in the case of a prototype where the main constraint is achieving self-oscillation using an Halbach array as a field source, and a La(Fe,Si)$_{13}$H plate as an active substance. Our system uses a geometry similar to the one studied in [3] with two main differences: the magnetic field lines are much more spatially confined, and the MCM is a first order material.
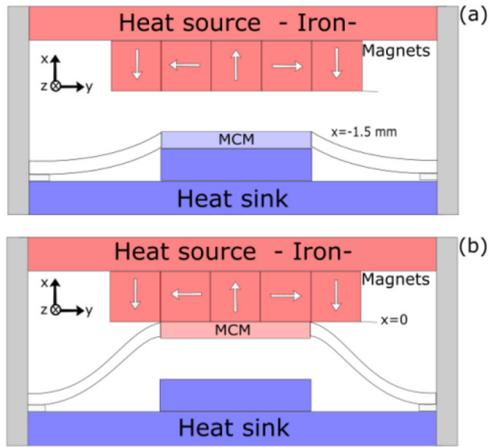
[*] e-mail: smail.ahmim@satie.ens-cachan.fr

Fig. 1. Thermomagnetic generator, (a) the MCM is in contact to the heat sink, (b) the MCM is in contact to the hot source.
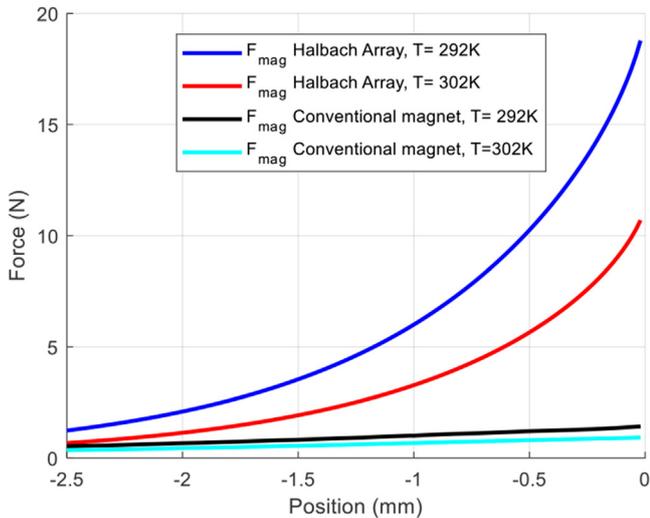

Fig. 2. Simulated magnetic force of a Halbach array and a single magnet with the same dimensions $(3 \times 10 \times 15\,\mathrm{mm}^3)$ at $T = 292\,\mathrm{K}$ and $302\,\mathrm{K}$.

In Section 2, we present our device design and work-out the self-oscillation conditions for the mechanical system. In Section 3, we focus on the mechanical-to-electrical energy conversion using two different techniques, one based on induction through micro-coils, the other using a piezoelectric transducer. In the conclusions, we discuss the results and foreseen some possible optimization strategies.

2 Operating principle and thermal to mechanical energy conversion

In our TMG a La-Fe-Si plate $(1 \times 6 \times 10\,\mathrm{mm}^3)$ moves between two heat reservoirs. Material data comes from Erasteel La(Fe,Si)$_{13}$H materials performed in a project (ANR MagCool Project). Thermal exchange takes place by contact (i.e. the MCM is both the refrigerant and the exchanger). The magnetic field is confined near the hot end
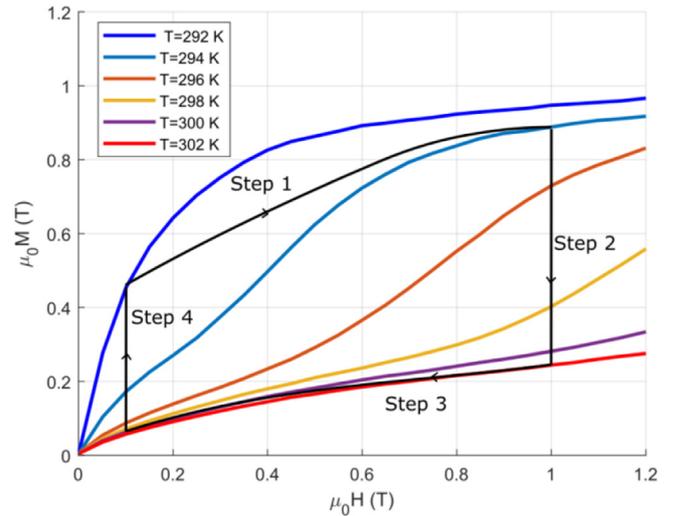

Fig. 3. Thermodynamic cycle in the M–H plane. Isothermal magnetization curves (temperature in the legend). The two adiabatic (Steps 1 and 3) and the two iso-field (Steps 2 and 4) transformations are represented.

thanks to a Halbach array, which is built using NdFeB parallelepiped magnets $(3 \times 3 \times 10\,\mathrm{mm}^3)$. The MCM is fixed in the middle of a polypropylene beam (see Fig. 1). The gap between the two heat sources is 1.5 mm.

Most TMG prototypes use single magnets [3,4]. Here, we use a Halbach array in order to increase the field spatial confinement and to reduce the demagnetizing fields. Moreover, the force is stronger and has a steeper change over small displacements than with a single magnet as shown in Figure 2. The forces in Figure 2 are estimated using a 3D finite element model (Maxwell from Ansys).

The generator carries out a Brayton cycle with two iso-fields and two adiabats (i.e. adiabatic transformations) as follows:

Step 1 – adiabat: the MCM starts in contact with the heat sink (see Fig. 1a). As the material is ferromagnetic, the magnetic force is larger than the return force of the spring (see Step 1, Fig. 4) and moves the plate towards the hot source. Along this movement the MCM is magnetized by the field spatial gradient and its temperature increases due to the magnetocaloric effect (see Step 1, Fig. 3). The displacement is fast enough to be considered adiabatic.

Step 2 – iso-field: the MCM is in contact with the hot source (see Fig. 1b), its temperature increases and the magnetization decreases (see Step 2, Fig. 3). As a result, the applied magnetic force decreases too (see Step 2, Fig. 4). The MCM receives a thermal flux from the heat source under constant applied magnetic field.

Step 3 − adiabat: the MCM still in contact with the heat source becomes paramagnetic. The return force of the spring overcomes the magnetic force (see Step 3, Fig. 4) and moves the plate towards the heat sink. During the displacement the MCM temperature decreases due to the adiabatic demagnetization. Again, the displacement along the field gradient is fast enough to consider the transformation adiabatic.
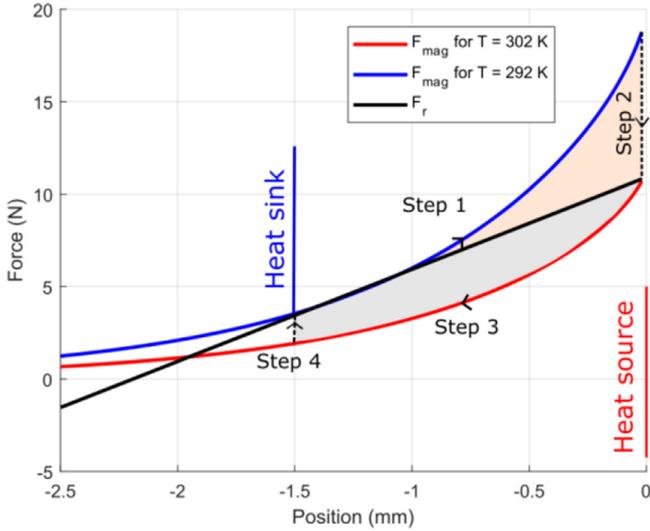
Fig. 4. Thermodynamic cycle represented on the force-displacement plane. Magnetic force (F_{mag}) at $T = 292\,\mathrm{K}$, $T = 302\,\mathrm{K}$ and return force of the beam (with open circuit piezoelectric elements) (F_r) as a function of position (x). The two adiabatic (Steps 1 and 3) and the two iso-field (Steps 2 and 4) transformations are represented. The light red and gray filled areas represent the energy available during the Steps 1 and 3.

Step 4 – iso-field: the MCM is in contact with the heat sink. It cools down and its magnetization increases (see Step 4, Fig. 3). The MCM transfers a thermal flux to the heat sink under a constant magnetic field (see Step 4, Fig. 3).

It is apparent from the description of the four steps that the electrical energy output will mostly concern the two adiabats (Steps 1 and 3). More precisely, it will take place exclusively along these two stages when using piezoelectric transducers. When using coils we can take into account also the magnetic flux change associated to the phase transition taking place along the iso-field transformations. However, this is a slow process and it is easy to show that it will be negligible with respect to the fast flux change associated with the adiabatic displacement.

Here, we focus on the fast processes, namely on the mechanic to electrical energy conversion, and we neglect slow thermal-exchange lead processes (iso-field transformations).

Our device is designed in order to reduce its dynamics into a one-dimensional equation of motion where only the vertical position of the moving part matters. As our goal is to achieve self-oscillation, we shall wisely balance the two forces acting on the MCM, namely the magnetic and the elastic one.

The magnetic force, $F_{\mathrm{mag}}(T, x)$, depends on temperature T through the magnetization, and on the field through the position of the plate with x the vertical position of the material ($x = 0$ and $x = -1.5\,\mathrm{mm}$ when in contact with the hot and the cold end respectively). To simplify numerical calculations, we assume that the magnetization change along the adiabats is mainly associated with position (i.e. field), neglecting the change of saturation magnetization due to the adiabatic temperature change.

This looks like a reasonable approximation as long as the phase transition takes place mostly during the iso-field transformations. On the other hand, the elastic return force, $F_r(x)$, depends on nothing but the position.

Figure 3 shows the magnetization of the LaFeSi versus the applied field for different temperature. Figure 4 shows the magnetic force applied on the MCM for 292 K and 302 K. As we expected, the magnetization (see, Fig. 3) and the magnetic force (see, Fig. 4) decreases with the temperature. The force is estimated using a 3D finite element model (Maxwell from Ansys).

To achieve the self-oscillation of the device, the cantilever beam must be designed in such a way that $F_{\mathrm{mag}}(292\,\mathrm{K}, -1.5\,\mathrm{mm}) > F_r(-1.5\,\mathrm{mm})$, $F_{\mathrm{mag}}(302\,\mathrm{K}, 0) < F_r(0)$, and the magnetic force slope must be greater than the elastic force one respectively at end of Steps 4 and 1 (see Fig. 4). The suitable beam stiffness is $k = 5900\,\mathrm{N/m}$.

3 Energy harvesting and mechanical to electrical energy conversion

In this section, we study the mechanical into electrical energy conversion. During Steps 1 and 3, the MCM acquires a certain amount of mechanical energy (the gray and light red areas in Fig. 4) due to the forces acting on it. The goal here is to recover as much as possible of this energy avoiding dissipation during the shock with the reservoirs.

An efficient transducer must be able to convert into electrical energy most of the mechanical work received. The energy balance between the mechanical work available, the kinetic energy and the energy harvested is given by the following expression:

$$\left(F_{\mathrm{mag}} - F_r\right)dx = d\left(\frac{1}{2}mv^2\right) + dW_{\mathrm{rec}} \qquad (1)$$

where m is the mass of the moving part (La(Fe,Si)$_{13}$H density is around $7.8\,\mathrm{g/cm^3}$), v its speed, and dW_{rec} corresponds to the work done by the transducer.

During the Steps 1 and 3, the mechanical work available is given by $\int \left(F_{\mathrm{mag}} - F_r\right)dx$ integrated along the displacement. It represents the light red filled area for Step 1 and the gray filled area for Step 3 on Figure 4.

Since, we are focusing on the Steps 1 and 3, parameters related to the whole thermodynamic cycle as the frequency [7] the electrical power, the thermal transfer [8] will not be treated. Our main point here is to study the ratio between the electrical energy harvested and the mechanical energy available.

Ideally, we would like to reduce the moving part speed to zero when the MCM gets in contact with the reservoirs, thus avoiding energy losses associated with the shock. However, this condition can hardly be achieved using a purely passive mode, that is when no voltage is applied to the transducers. This goal could be achieved switching to an active mode by applying a voltage on the transducers in order to induce a gradual deceleration of the MCM. In the following, we study the conversion using coils and piezoelectric transducers in the passive mode.
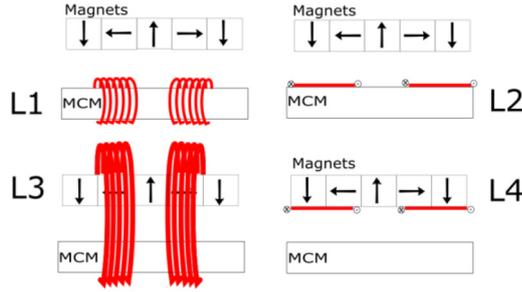
Fig. 5. Different coil positions. L1, coils placed around the MCM. L2, coils placed on the MCM. L3, coils placed around the structure. L4, coils are placed under the magnets.

3.1 Estimation of the recoverable mechanical energy using coils

Using coils allows to pick-up the global magnetic flux change, either due to the MCM displacement (i.e. kinetic energy), or to the magnetization change during the phase transition. However, as pointed out above, the latter is negligible compared to the former.

The induced voltage $u(t)$ at the coil is given by:

$$u(t) = \frac{d\emptyset}{dt} = pv(t) \int_0^{L_i} \frac{dB}{dx} dl \qquad (2)$$

where p is the depth, $\frac{d\emptyset}{dt}$ the flux rate of change and L_i the length of L1, L2, L3 and L4 (see Fig. 5). The power received by the external load is:

$$P_{\text{load}}(t) = \frac{R_{\text{load}}}{(R_{\text{load}} + R_{\text{coil}})^2} u(t)^2 \qquad (3)$$

where R_{load} is the external load resistance, and R_{coil} is the internal resistance of the coil. The self-induction of the coil is neglected. At maximum power, i.e. $R_{\text{load}} = R_{\text{coil}}$, the power received by the load is half the power provided by the generator.

$$P_{\text{load}}^{\max}(t) = \frac{u(t)^2}{4R_{\text{coil}}}. \qquad (4)$$

Through R_{coil}, we see that the power harvested depends on the volume of wire, V_{copper}, with

$$P_{\text{load}}^{\max}(t) = \left(\frac{d\emptyset}{dt}\right)^2 \frac{S}{4\rho L} = \left(\frac{d\emptyset}{dt}\right)^2 \frac{V_{\text{copper}}}{4\rho L^2} \qquad (5)$$

where S is the section of a single coil, L the length of a single coil and ρ the resistivity of the copper. $P_{\text{load}}^{\max}$ is computed by using equation (5) where $\frac{d\emptyset}{dt}$ is calculated using equation (2) where the speed $v(t)$ and $\frac{dB}{dx}$ are derived respectively from solving the equation of dynamics and FEM calculation. The MCM's speed and the volume of wire are the main parameters to improve the power. Once, we have the maximum power, the recovered energy E_r is calculated

Table 1. The ratios of energy recovered (E_r) for the coils L1, L2, L3 and L4 over the mechanical energy (E_a). $E_a = 116\,\text{mJ}$ per $1\,\text{cm}^3$ of the MCM.

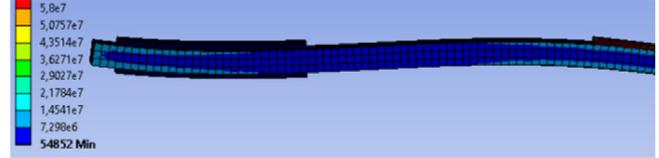| Coil	$E_r/E_a(\%)$
L1	0.0085
L2	0.018
L3	0.0065
L4	0.006

Fig. 6. The bending energy recovery system. The system being symmetrical, only a part has been represented. The equivalent constraints of Von-Mises are represented. The stresses in the piezoelectric are of the order of 50 MPa.

using equation (6)

$$E_r = \frac{1}{t_{\text{switch}}} \int P_{\max}(t) dt \qquad (6)$$

where t_{switch} is the time needed for the MCM to reach the heat source or the heat sink.

Many configurations of coils are considered as shown in Figure 5. According to our manufacturing process, the copper thickness is $70\,\mu\text{m}$ with a square section. The length varies depending on the position of the coil.

Table 1 shows the ratios between recovered and mechanical energy, E_r/E_a, for the different configurations. The recovered energy E_r is computed using equation (6), and E_a the total mechanical energy available is given by $\int F_{\text{mag}}(T = 292\,\text{K}) - F_{\text{mag}}(T = 302\,\text{K})dx$.

The best performing coil position is L2 with $21\,\mu\text{J}$ per $1\,\text{cm}^3$ of the MCM. However, the maximum value reached remains relatively low; this can be explained by the low volume of the conductor compared to the energy to be converted.

It is also possible to improve the recovered energy by increasing the copper volume as apparent from equation (5). However, the volume cannot be significantly increased without considering the effect that its increase would have on the thermal behavior of the system.

3.2 Estimation of the recoverable mechanical energy using piezoelectric elements

Here, we study the energy harvester using piezoelectric materials with a 3D finite element model (Ansys). We choose a configuration where four piezoelectric patches are bonded to a polypropylene beam (see Fig. 6). For the piezoelectric patches, we use the PZT 5a parameters [9]. Each patch is 20 mm wide, 10 mm long and 3 mm thick.

The energy produced by a piezoelectric patch is estimated using the following formula [10]:

$$E = \frac{1}{2}CV^2 = \frac{1}{2}\frac{\varepsilon_0 \varepsilon_r L_p b_p}{h_p}V^2 \qquad (7)$$

where V is the generated voltage in an open circuit, ε_r the relative permittivity and h_p the thickness of the patch. V is directly worked-out by simulation, in our case $9.3\,\mathrm{V}$. With the four patches, the energy harvested is around $1.73\,\mu\mathrm{J}$ which corresponds to an energy density of $30\,\mu\mathrm{J/cm}^3$, value in agreement with the value found in [10].

4 Discussion and conclusions

In this study, we have discussed some roads towards thermomechanical conversion in a TMG device. We propose a design of the spring (i.e. the key component of our conversion chain) to achieve self-oscillation condition of the system. Afterwards we present numerical simulations to define the best options for the following conversion step, the one from mechanical to electrical energy. We find the optimal coil position when using Faraday law to recover electrical energy. In this case, the recovered energy is $21\,\mu\mathrm{J/cm}^3$, which represents 0.018% of the available mechanical energy $(116\,\mathrm{mJ/cm}^3)$. Further simulations using piezoelectric materials give similar orders of magnitude for the efficiency, with a recovered energy of $30\,\mu\mathrm{J/cm}^3$, which represents only 0.025% of the available energy, still a tiny fraction indeed.

In the case of the coils, we can improve the recovered energy by increasing the volume of the copper (see Eq. (5)). Many parameters are limiting this volume as for instance the reduced space between the two heat sources. We can also improve the recovered energy by increasing $\frac{d\phi}{dt}$. We shall devote further efforts to this option. The piezoelectric elements recover more energy than the coils but the efficiency is still rather low. To be more efficient the transducers should apply a force of the same order of magnitude as the magnetic one. For the piezoelectric transducers, the recovered energy can be optimized by tuning the sizes of the patches. However, our simulations show that even doing that we shall hardly get above a 0.034% recovery efficiency. We shall consider changing the beam material (e.g. Cu-2% Be rather than polypropylene) in order to improve the constraints on the piezoelectric elements.

Author contribution statement

S. Ahmim performed all the simulations and wrote the manuscript. A. Pasko and F. Mazaleyrat worked on the MCM caracterization. M. Almanza and M. LoBue supervised the project and worked on the manuscript. All the authors were involved on providing interpretations on the results and approved the final manuscript.

References

1. C. Forman, I.K. Muritala, R. Pardemann, B. Meyer, Estimating the global waste heat potential, Renew. Sustain. Energy Rev. **57**, 1568 (2016)
2. N.S. Hudak, G.G. Amatucci, J. Appl. Phys. **103**, 101301 (2008)
3. M.Ujihara, G.P. Carman, D.G. Lee, Appl. Phys. Lett. **91**, 093508 (2007)
4. M. Gueltig et al., Adv. Energy Mater. **7**, 1601879 (2017)
5. M. Almanza, A. Pasko, F. Mazaleyrat, M. Lobue, IEEE Trans. Magn. **53**, 1 (2017)
6. J.H. Cho, R.F. Richards, D.F. Bahr, C.D. Richards, M.J. Anderson, Efficiency of energy conversion by piezoelectrics, Appl. Phys. Lett. **89**, 104107 (2006)
7. M. Almanza, A. Pasko, F. Mazaleyrat, M. LoBue, Numerical study of thermomagnetic cycle, J. Magn. Magn. Mater. **426**, 64 (2017)
8. M. Almanza, L. Depreux, F. Parrain, M. LoBue, Electrostatically actuated thermal switch device for caloric film, Appl. Phys. Lett. **112**, 083901 (2018)
9. https://bostonpiezooptics.com/ceramic-materials-pzt (accessed 2018)
10. A. Rendon, S. Basrour, L. Tima, A.F. Viallet, JNRDM, 6 (2016)